

RESEARCH ARTICLE

A Diaphanous and Enabled-dependent asymmetric actin cable array repositions nuclei during *Drosophila* oogenesis

Gregory Logan, Wei-Chien Chou and Brooke M. McCartney*

ABSTRACT

Cells reposition their nuclei for diverse specialized functions through a wide variety of cytoskeletal mechanisms. During *Drosophila* oogenesis, 15 nurse cells connected by ring canals to each other and the oocyte contract, ‘dumping’ their cytoplasm into the oocyte. Prior to dumping, actin cables initiate from the nurse cell cortex and elongate toward their nuclei, pushing them away from ring canals to prevent obstruction. How the cable arrays reposition nuclei is unknown. We found that these arrays are asymmetric, with regional differences in actin cable growth rate dependent on the differential localization of the actin assembly factors Enabled and Diaphanous. Enabled mislocalization produces a uniform growth rate. In oocyte-contacting nurse cells with asymmetric cable arrays, nuclei move away from ring canals. With uniform arrays, these nuclei move toward the adjacent ring canal instead. This correlated with ring canal nuclear blockage and incomplete dumping. Our data suggest that nuclear repositioning relies on the regulated cortical localization of Diaphanous and Enabled to produce actin cable arrays with asymmetric growth that push nuclei away from ring canals, enabling successful oogenesis.

KEY WORDS: *Drosophila*, Oogenesis, Actin cables, Nuclear positioning, Enabled, Diaphanous

INTRODUCTION

Diverse cytoskeletal-based mechanisms underlie the regulated nuclear movement that occurs in a wide variety of cells. Many contexts employ microtubule pushing or pulling forces, including nuclear movement in yeast (Gundersen and Worman, 2013), during muscle development (Azevedo and Baylies, 2020) and nuclear repositioning in *Drosophila* oocytes (Tissot et al., 2017). Actin also repositions nuclei via varied mechanisms, including actomyosin contraction during neuronal migration (Nakazawa and Kengaku, 2020) and Myosin-based coupling to actin cables that relocates nuclei in migrating cells (Zhu et al., 2018). The nurse cells that drive *Drosophila* oogenesis use a unique mode of nuclear repositioning: enormous arrays of actin cables that can extend 30 µm or more push and relocate nuclei during stage 10B, a late stage of oogenesis (Cant et al., 1994; Guild et al., 1997; Huelsmann et al., 2013; Mahajan-Miklos and Cooley, 1994). Although this actin cable-driven nuclear movement has been described previously (Huelsmann et al., 2013), how the cable arrays reposition nurse cell nuclei is unknown.

The developing *Drosophila* oocyte is ‘nursed’ by 15 nurse cells connected to each other and the oocyte by actin-based ring canals (Fig. 1A). Stage 10B is defined by the movement of the centripetal cells between the oocyte and the nurse cells, and at this stage the entire nurse cell-oocyte cluster is surrounded by a layer of squamous and columnar follicle cells (Fig. 1A’). Through the ring canals, nurse cells send mRNAs, proteins and organelles into the oocyte, and together with vitellogenesis, this increases the volume of the oocyte by ~90,000-fold (King, 1971). During stage 11, nurse cell cortical contraction rapidly expels their remaining cytoplasm through the ring canals and into the oocyte, roughly doubling the oocyte size (Fig. 1A’). Immediately before this cytoplasmic ‘dumping’, striking arrays of cytoplasmic actin cables begin polymerizing at the nurse cell cortex, growing inward to contact the nurse cell nuclei (Guild et al., 1997, Fig. 1A’). These actin cables are highly ordered bundles of bundles of filaments: small 2–4 µm unit bundles containing ~26 parallel filaments are bundled together in an overlapping pattern to form mature cables (Guild et al., 1997). Without the cable arrays, as in mutants of the actin bundlers Singed/Fascin (Cant et al., 1994) and Quail/Villin (Mahajan-Miklos and Cooley, 1994), nuclei clog the ring canals during dumping, preventing the completion of oogenesis. Live imaging revealed that the actin cables push and roll the nuclei away from the ring canals as dumping commences (Huelsmann et al., 2013). In addition to the exquisite temporal control of cable assembly, the repositioning of nuclei away from ring canals also suggests spatial control; if cables initiated simultaneously and grew at an equivalent rate from all surfaces of the nurse cell cortex, the nuclei might remain static. This model predicts that the actin cable array has additional regulated temporal and/or spatial asymmetries to promote robust nuclear relocation away from the ring canals.

Nurse cells share ring canals with adjacent nurse cells and with the oocyte, but not with follicle cells (Fig. 1A). The actin cables are exclusively in nurse cells and, for simplicity, we will refer to different populations of cables based on whether the cable originates from a region of the nurse cell cortex adjacent to the follicle cells, the oocyte or another nurse cell (Fig. 1B,C). Some nurse cells have all cable types, and others only have nurse cables and follicle cables, depending on their position within the cluster (Fig. 1B). We found that although nurse cables and oocyte cables are both fast growing, follicle cables are significantly slower. We show that this asymmetry in cable growth rate correlates with the distribution of the actin elongation factor Enabled (Ena); Ena localizes to the nurse cell cortex but is excluded from the cortex where follicle cables grow. In contrast, the formin Diaphanous (Dia) localizes to the nurse cell cortex at all interfaces. This suggests that Ena and Dia collaborate to assemble nurse cables, while follicle cables depend solely on Dia. Consistent with that prediction, reduction of Dia impacted the initiation and elongation of both nurse cables and follicle cables, while Ena was necessary for only nurse cable initiation and elongation. Mislocalization of Ena to the

Department of Biological Sciences, Carnegie Mellon University, 4400 Fifth Avenue, Pittsburgh, PA 15213, USA.

*Author for correspondence (bmccartney@cmu.edu)

DOI: 10.1242/dev.197442; G.L., 0000-0002-4428-1807; B.M.M., 0000-0002-5071-8550

Handling Editor: Thomas Lecuit

Received 1 October 2020; Accepted 24 May 2022

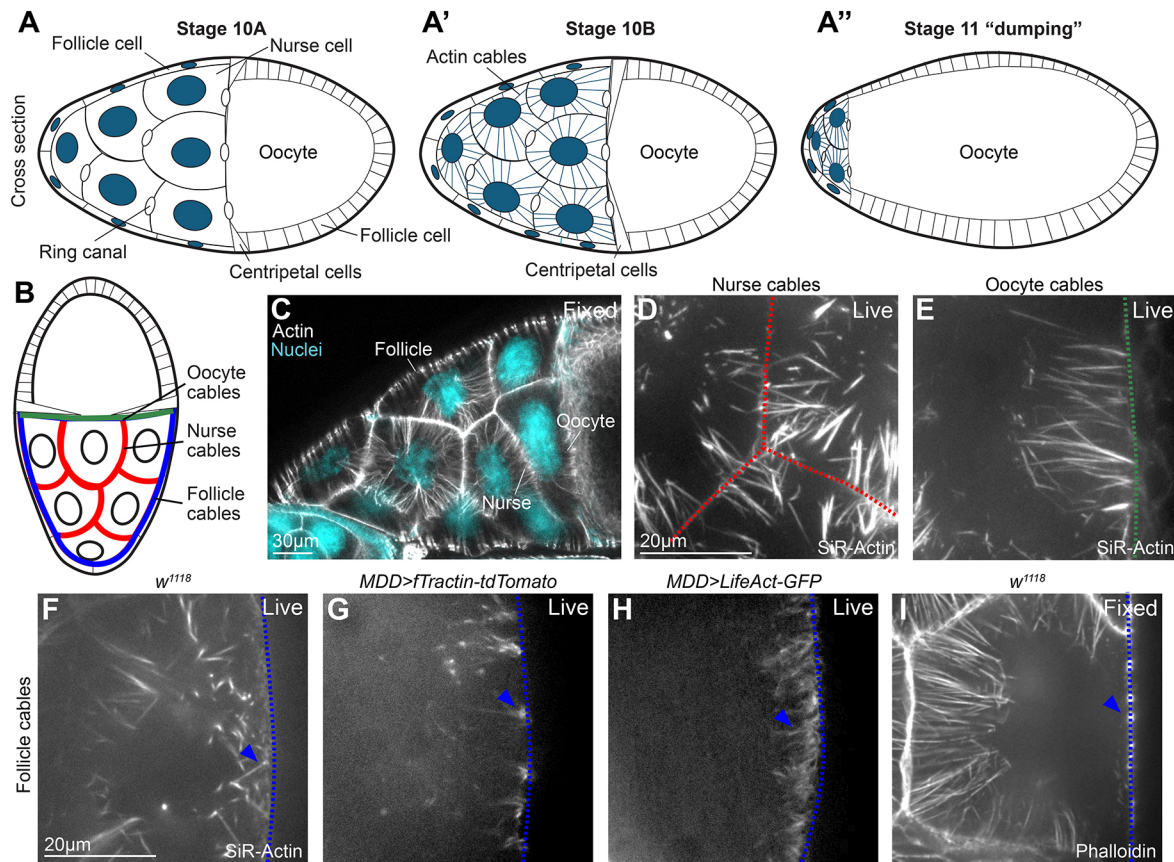


Fig. 1. Stage 10B *Drosophila* nurse cells extend actin cables from all regions of the cortex. (A-A'') Schematic of stage 10-11 egg chambers. (B) Schematic of the location of the three nurse cell cable types, designated by the type of cell that the nurse cell borders. (C) A fixed *w¹¹¹⁸* (wild-type) egg chamber showing the positions of the three nurse cell cable types. (D-I) Colored lines correspond to those in B. (D,E) Live images of SiR-Actin labeled nurse cables (D) and oocyte cables (E). (F-H) Live images of follicle cables labelled with SiR-Actin (F), fTractin-tdTomato (G) and LifeAct-GFP (H). (I) Image of a fixed *w¹¹¹⁸* egg chamber preserving no follicle cables. All experiments were replicated at least three times.

nurse cell cortex adjacent to the follicle cells eliminated the asymmetry in cable growth rate producing a uniformly fast-growing actin cable array. We tracked the movement of nuclei in nurse cells adjacent to the oocyte in late stage 10B and found that with wild-type asymmetric arrays, the nuclei generally move toward the nurse cell cortex bordering the follicle cells. With uniform arrays, the nuclei instead move toward the anterior nurse cell where there is a ring canal connecting the two nurse cells. A uniform actin cable array was also associated with nuclear blockage of ring canals and incomplete dumping.

Our data suggest that the differential localization of Ena and Dia is a key regulatory mechanism governing the asymmetry in cable growth rate. Furthermore, our results support the model that cable growth rate asymmetry is necessary for the proper repositioning of the nurse cell nuclei and the successful completion of oogenesis.

RESULTS

Nurse cables, oocyte cables and follicle cables exhibit a peak of initiation early in stage 10B and have similar densities

Using phalloidin to label fixed tissue and/or three different probes to detect actin in live tissue (SiR-Actin, and genetically encoded fTractin-tdTomato or LifeAct-GFP), we identified all types of actin cables at stage 10B (Fig. 1C-I). As in previous studies (Huelsmann et al., 2013), we found no actin cables on the follicle cell side of

fixed nurse cells (Fig. 1C,I), suggesting that follicle cables are sensitive to fixation. Actin cable fixation sensitivity has been observed in other systems (Vasicova et al., 2016). Although we visualized cables at all nurse cell interfaces using all three live imaging probes, we chose SiR-Actin for our experiments because it did not appear to induce any obvious changes to the actin cable array. In contrast, fTractin-tdTomato labelled actin cables had clusters of fluorescence at the base of each cable (Fig. 1G, arrowhead) that we did not observe with SiR-Actin, LifeAct-GFP or fixed. LifeAct-GFP appeared to induce higher densities of follicle cables (Fig. 1H; Spracklen et al., 2014a) compared with SiR-Actin or fTractin-tdTomato.

To understand the dynamics and composition of the actin cable array, we examined actin cable initiation rate and density in different parts of the array. We were unable to image stage 10A egg chambers prior to any cable initiation (Fig. 1A), as these fail to progress *ex vivo* (Spracklen and Tootle, 2013). Consequently, we isolated stage 10B egg chambers for imaging with SiR-Actin and selected for analysis those at the earliest points of cable initiation at the start of imaging. Individual *w¹¹¹⁸* (wild type) egg chambers were imaged for a maximum of 90 min. Within a single nurse cell, we observed differences in the timing of initiation that depended on the z-axis position: deeper nurse cables (Fig. 2A'-C', arrowhead) initiated before more superficial cables (Fig. 2A-C, arrowhead). To assess initiation rate (Fig. 2D,D'), we measured the number of new cables (<3 μm long) per μm of membrane at each time point. For all cable

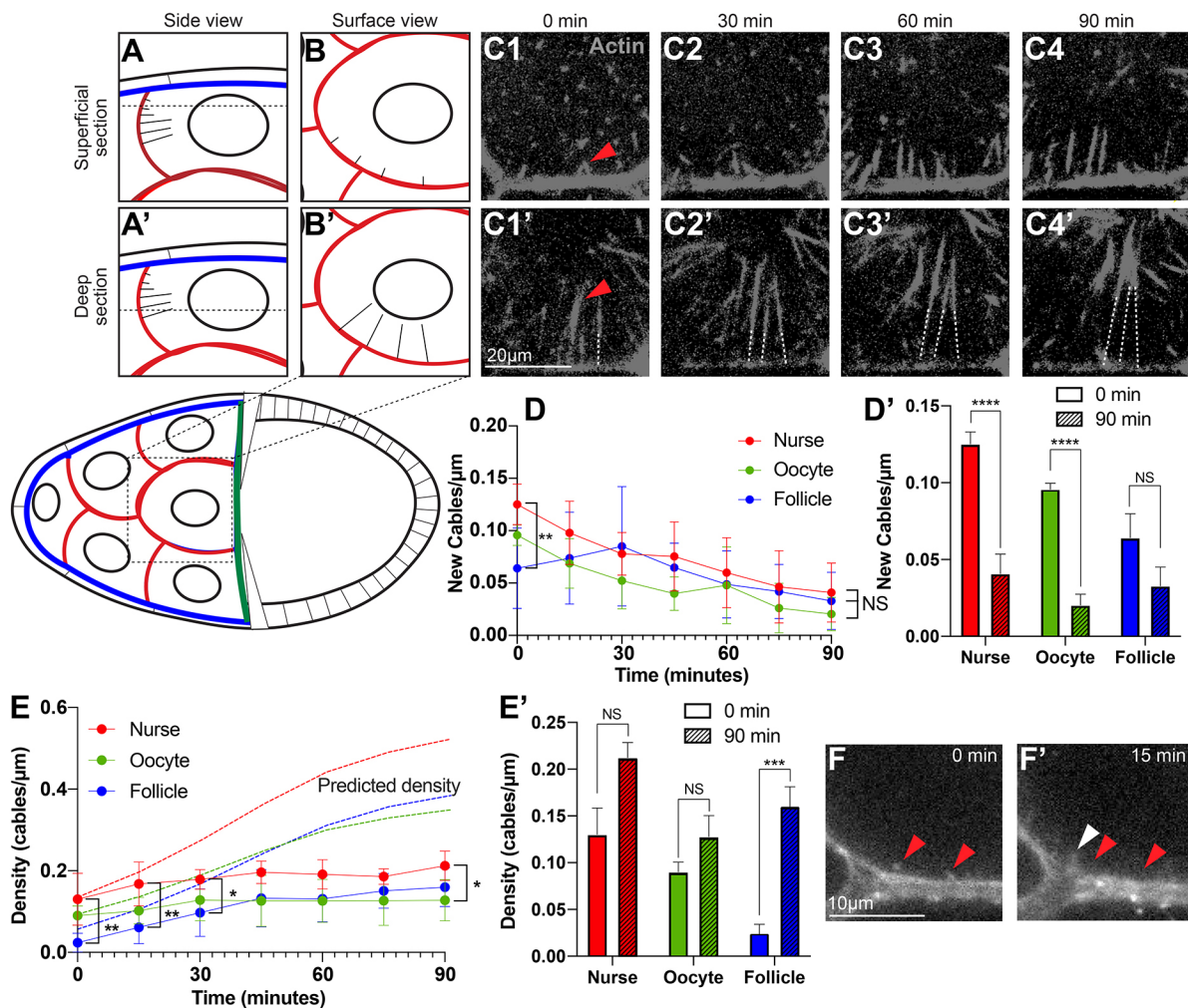


Fig. 2. Different cable types exhibit minimal differences in initiation rate and density. (A,B) Schematics of cables initiating from a superficial section of a nurse cell, closer to the follicular epithelium, in cross section (A) and in surface view (B), or cables initiating from a deeper section (A',B'). Cable outgrowth shown in a live imaging series from a superficial section (C1-C4, arrowhead) or from a deeper section (C1'-C4', arrowhead). As cables elongate, they often cross z-planes, leading to apparent gaps near the cortex (dashed lines). (D) Cable initiation rate, measured as number of new cables ($<3 \mu\text{m}$ long) per μm of membrane at each timepoint starting at the beginning of stage 10B. (D') Comparisons of cable initiation rate at the beginning (0 min) and end (90 min) of imaging. (E) Actual (solid lines) and predicted (dashed lines) actin cable density over time. (E') Comparisons of actual cable density at the beginning (0 min) and end (90 min) of imaging. (F) Some nurse cables initiate but appear to disassemble (red arrowheads). The white arrowhead indicates a newly initiating cable. n =number of egg chambers. All experiments were replicated at least three times and data are shown as mean \pm s.e.m. (D,E) One-way ANOVA with Tukey's post-hoc analysis, $n=6$. (D',E') Two-way t -test, $n=6$. * $P<0.03$, ** $P<0.002$, *** $P<0.0002$, **** $P<0.0001$.

types, the largest number of new cables appeared at the beginning of stage 10B (Fig. 2D), but initiation did not stop completely during the first 90 min (Fig. 2D,D'). At time 0, the cable initiation rate was significantly higher for nurse cables compared with follicle cables, but by 90 min the rate of new cable emergence was similar for all three cable types (Fig. 2D). Based on that initiation pattern, we predicted that the cable density would significantly increase over time (Fig. 2E, dotted lines). Surprisingly, although there was a trend toward increased cable density (Fig. 2E, solid lines), it only increased significantly for follicle cables (Fig. 2E'). The dramatic difference between predicted and observed cable density is likely because some cables that initiate fail to elongate (Fig. 2F,F', red arrowheads). Although there were some significant differences in cable density between the three cable types over the imaging period, by 90 min they were similar (Fig. 2E). Taken together, we observed some minor differences between the cable types in the rate of initiation and density, but overall these characteristics were very similar.

Follicle cables grow slower and contact the nucleus later than nurse and oocyte cables

Because cables grow from all nurse cell cortices, we predicted that the different populations of cables would exhibit different growth rates to enable the cables to reposition the nuclei away from the ring canals during dumping. To test this, we measured the growth rate of each population during early cable growth in w^{1118} nurse cells (e.g. Movie 1). Nurse and oocyte cables had a virtually identical average growth rate of $0.11 \mu\text{m}/\text{min}$ (Fig. 3A,B). We observed the same growth rate for cables labelled with fTractin-tdTomato (Fig. S1A,B). This was significantly faster than follicle cables, which grew at $0.07 \mu\text{m}/\text{min}$ (Fig. 3A,B). Stage 10B lasts for ~ 4 h, during which time the cables emerge and contact the nucleus. Therefore, we sampled the entire growth period in 90 min increments and integrated the data (see Materials and Methods) for the nurse cables (representative of the faster growing cables) and the follicle cables to determine whether the growth rate changed over time (Fig. 3C). Both nurse cables and follicle cables maintained a constant growth

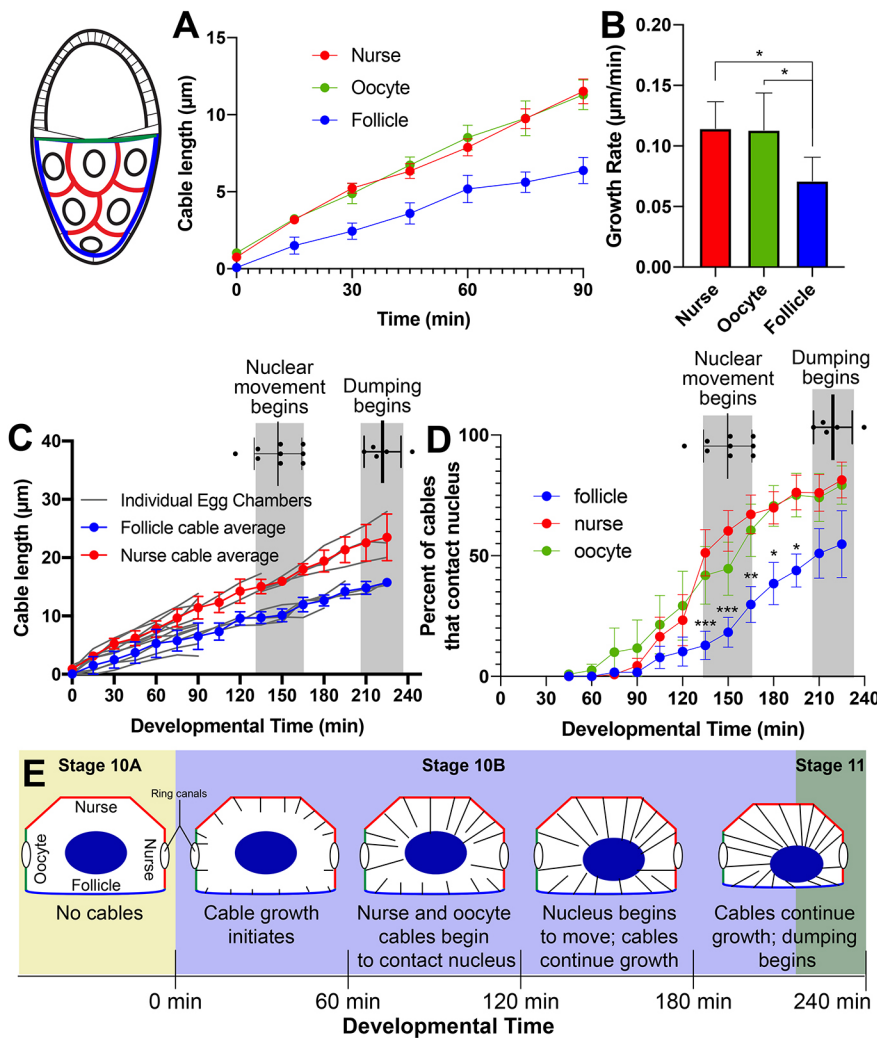


Fig. 3. Cable types exhibit significant differences in growth rate and nuclear contact in wild-type nurse cells. (A,B) Follicle cable growth rate is significantly slower than that of nurse or oocyte cables. (A) Nurse, oocyte and follicle cable length over the first 90 min of stage 10B. (B) Cable growth rates. One-way ANOVA, $n=6$. (C) Nurse cable and follicle cable growth over the 4 h of stage 10B, showing consistent growth rates throughout. (D) Percentage of cables that contact nuclei over time. A significantly higher percentage of oocyte and nurse cables are in contact with nuclei when they begin to move (first gray bar) compared with follicle cables. One-way ANOVA, $n=10$. (E) Synopsis of actin cable growth through stage 10B, illustrating the differences in growth rate and nuclear contact. Nuclear movement trajectory is predicted. * $P<0.03$, ** $P<0.002$, *** $P<0.0002$, Tukey's post-hoc analysis. n =number of egg chambers. All experiments were replicated at least three times and data are mean \pm s.e.m.

rate throughout stage 10B (Fig. 3C). Nurse cell nuclei initiated movement between ~135 and 175 min with dumping initiating between 210 and 240 min (Fig. 3C, shaded bars). Thus, both cable types grew at a constant rate from initiation through dumping.

Cables began to contact the nucleus 75–105 min after the start of stage 10B, with a steady increase between 120 min and ~240 min (Fig. 3D). As nuclear movement began, the percent of nurse cables and oocyte cables contacting the nucleus was significantly higher than that of follicle cables (Fig. 3D). This suggests that the movement of the nuclei is primarily due to the activity of the nurse and oocyte cables. Taken together, our data demonstrate that cable growth rates and the timing of nuclear contact differ between different populations of actin cables. Nurse cables and oocyte cables, those that grow from the part of the cortex where the ring canals reside, grow faster and contact the nurse cell nuclei in greater numbers as the nuclei are moving than the slower growing follicle cables. These results suggest that spatial asymmetry in cable growth and nuclear contact repositions the nuclei away from the ring canals prior to dumping (Fig. 3E).

Dia and Ena differentially localize to the nurse cell cortex

Our model of actin cable growth is based largely on the electron microscopy of Tilney and colleagues, and suggests that actin assembly factors at the nurse cell cortex produce 2–4 μm actin filaments that are bundled into cable units that are then

bundled into growing cables (Guild et al., 1997). The spatial differences in cable growth rates that we observed suggest that different actin assembly factors may be responsible for nucleating and elongating the faster growing nurse and oocyte cables, and the slower growing follicle cables. The single *Drosophila* Ena/VASP family filament elongating protein Ena is required for at least some actin cable growth in nurse cells (Gates et al., 2007) and interacts with the formin Dia *in vitro* and *in vivo* (Bilancia et al., 2014). Both Dia and Ena can independently promote filopodia formation, a structurally similar actin cable, but the dynamics and morphologies of those filopodia differ (Barzik et al., 2014; Bilancia et al., 2014; Homem and Peifer, 2008, 2009; Nowotarski et al., 2014).

At stage 10B, we found that both Dia (Fig. 4A2,B2, red arrowheads) and Ena (Fig. 4A3,C3, red arrowheads) were enriched at the nurse cell cortex adjacent to other nurse cells (Fig. 4D,E) and adjacent to the oocyte (Fig. 4J,K, green arrowheads), i.e. sites of fast-growing cables. In contrast, Dia (Fig. 4A2,C2,D, blue arrowheads), but not Ena (Fig. 4A3,C3,E, blue arrowheads), localized to the nurse cell cortex adjacent to the follicle cells where slower growing follicle cables are found. Comparison of cortical to cytoplasmic ratios at these two regions of cortex support the conclusion that Dia and Ena are similarly enriched at nurse cell borders, but only Dia is significantly enriched at follicle cell borders (Fig. 4F). Although the anti-Dia antibody cannot distinguish

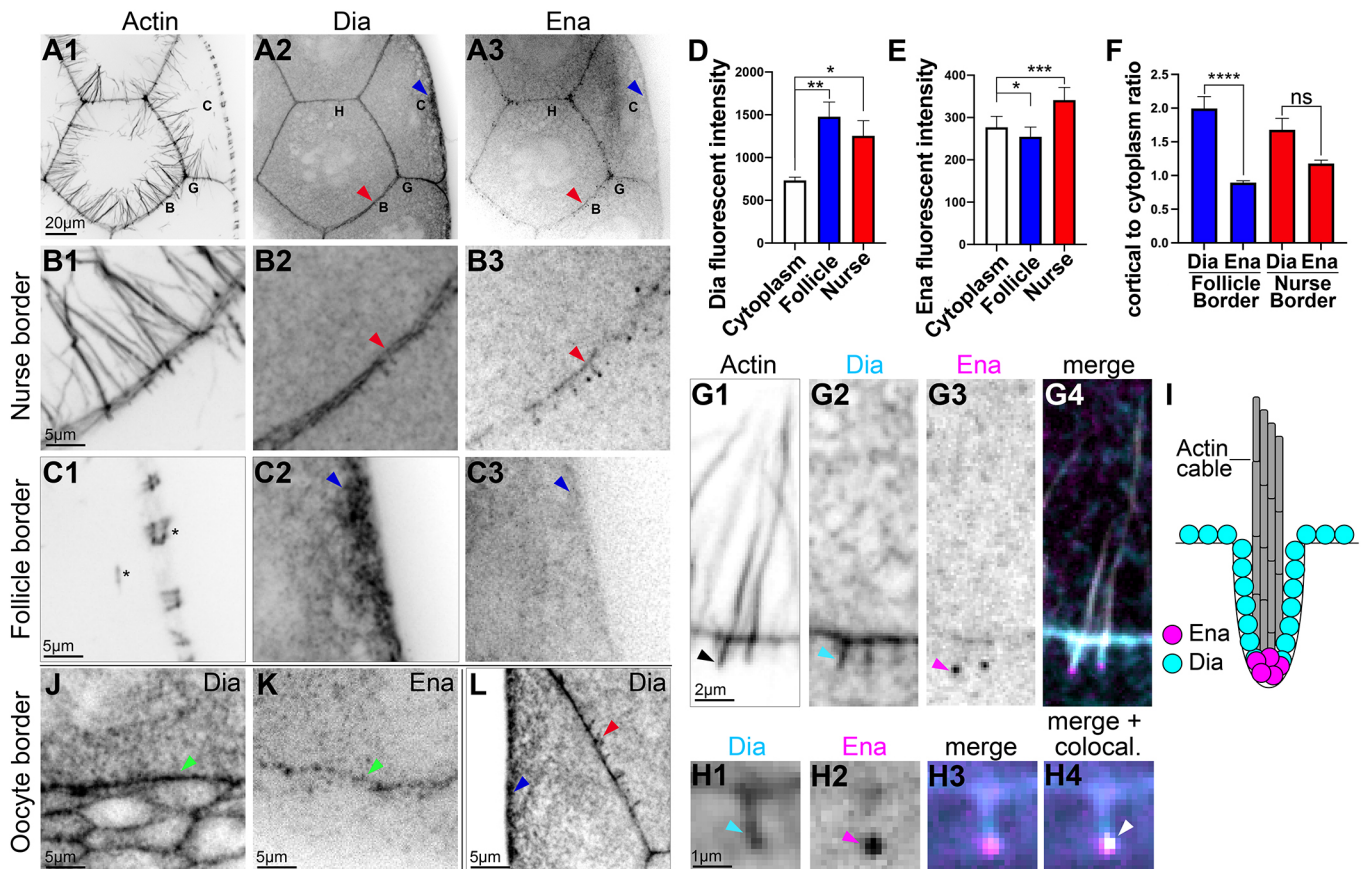


Fig. 4. Ena and Dia have both overlapping and distinct localization patterns at the nurse cell cortex. All tissue is *w¹¹¹⁸* (wild type). (A1–C3) Projections of five optical slices with a 0.2 μ m step size. (C1) The muscle sheath surrounding the egg chamber and fragments of an actin cable originating from another region of the cortex are labeled (asterisks). (A1–F) Dia is enriched at all regions of the nurse cell cortex, while Ena is excluded from the cortex bordering the follicular epithelium. Lettered areas in A1–A3 are magnified in B1–B3, C1–C3, G1–G3 and H1–H3, as indicated. Dia is enriched at the nurse cell cortex at both nurse cell–nurse cell borders (A2, B2, red arrowheads), and at nurse cell–follicle cell borders (A2, C2, blue arrowheads). Ena is enriched at the nurse cell cortex at nurse cell–nurse cell borders (A3, B3, red arrowheads), but not at nurse cell–follicle cell borders (A3, C3, blue arrowheads). Quantification of Dia (D) and Ena (E) fluorescent intensity at the cortex as indicated compared with their fluorescent intensity in the cytoplasm. (F) Comparison of Dia and Ena cortical enrichment as indicated. (G1–G4) Ena and Dia localize to the actin cable pits (arrowheads). G2 and G3 are single optical sections and G1 is a projection of two optical slices to capture the distal ends of the actin cables. (H1–H4) Some Dia (H1, arrowhead) colocalizes with Ena (H2, arrowhead) in the tip of the cable pit. Colocalized pixels are shown in white (H4, arrowhead). (I) Schematic of Dia, Ena and actin localization in pits based on the images in G and H. Dia (J) and Ena (K) localize to the nurse cell–oocyte border (green arrowheads). (L) Dia localizes to pits at nurse cell–nurse cell borders (red arrowhead), but no pits were observed at nurse cell–follicle cell borders (blue arrowhead). (D–F) One-way ANOVA, $n=6$. * $P<0.03$, ** $P<0.002$, *** $P<0.0002$, **** $P<0.0001$ Tukey's post-hoc analysis. n =number of egg chambers. All experiments were replicated at least three times and data are mean \pm s.e.m.

between active and inactive Dia, these results suggest that Dia may assemble filaments independent of Ena to produce the slower growing follicle cables, while the faster growing cables are the result of the combined activity of Dia and Ena. To examine this possibility further, we asked whether and how Dia and Ena colocalize at the nurse cell cortex. The barbed (growing) ends of the cables are often found in membrane evaginations or ‘pits’ protruding into neighboring nurse cells (Fig. 4G,H, arrowheads; Gates et al., 2009). The function of these cable pits is unknown. Ena is prominently localized at the base of these pits (Fig. 4G3,H2, arrowheads, G4, H3,4; Gates et al., 2009), similar to its localization in the filopodial tip complex (Leijnse et al., 2015). Dia is largely uniform at the nurse cell cortex (Fig. 4B2,G2), but also localizes to cable pits (Fig. 4G–I). Here, Dia is found along the shaft without Ena (Fig. 4G2, H1, arrowheads), but can also be found overlapping with Ena in the pit tip (Fig. 4H4, arrowhead). Ena and Dia exhibit a similar spatial relationship in some filopodia (Bilancia et al., 2014). On the follicle cell side of the nurse cell cortex, we did not find any evidence of cable pits (Fig. 4L, blue arrowhead). Based on these results, we

predict that the differential localization of Dia and Ena may be responsible for the differences in cable growth rates.

Reduction of Dia decreases nurse cable and follicle cable density, and reduces or halts cable growth

Our localization data suggested that Dia might be necessary for the growth of all cable types. To test this, we reduced Dia in nurse cells by expressing two different *UAS-dia-dsRNA* transgenes using *MDD-GAL4* (*MDD*>; germline driver). Anti-Dia fluorescence was significantly reduced at both nurse cell and follicle cell borders in tissue expressing either *dia-dsRNA* transgene (Fig. S2A–E). Stronger Dia reduction using *MTD-GAL4* (*MTD*>; germline driver) blocked oogenesis prior to stage 10B. Consistent with our hypothesis, reduction of Dia resulted in a significant loss of both nurse and follicle cables (Fig. 5A–D,H). The remaining nurse cables often clustered (Fig. 5B,C, arrowheads) and exhibited growth defects (Fig. 5E). With both dsRNAs, approximately half of egg chambers had cables with a wild-type growth rate, while the other half had slower growing or completely stalled cables (Fig. 5E–G,

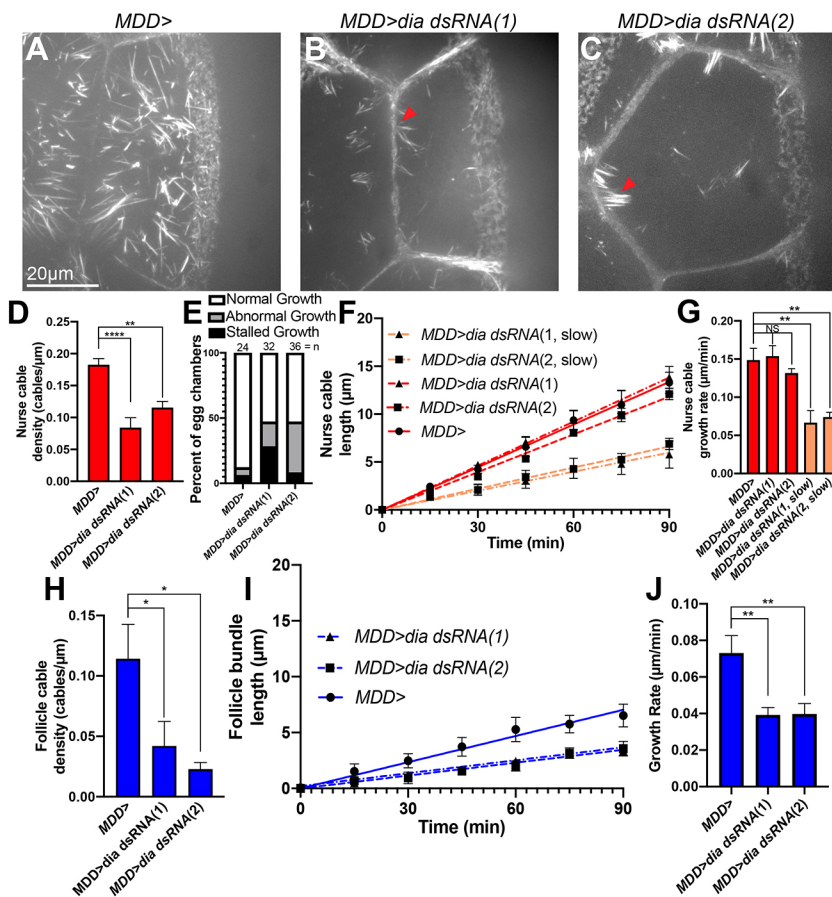


Fig. 5. *Dia* is required for normal nurse cable and follicle cable initiation and growth rate.

(A-C) Representative live images of actin cables in control (A) and in two partial *dia-dsRNA* knockdown egg chambers (B,C) showing decreased cable density and clustered cables in the *dia* knockdown (arrowheads). (D) Quantification of nurse cable density. (E) Categorization of egg chamber growth phenotypes in genotypes as indicated. (F,G) Nurse cable length over time in control and *dia-dsRNA* egg chambers. A subset of nurse cables in *dia-dsRNA* egg chambers grow significantly slower than in the control. (H) The follicle cable density is significantly lower in *dia-dsRNA* egg chambers. (I,J) Follicle cable length over time in control and *dia-dsRNA* egg chambers. All follicle cables in *dia-dsRNA* egg chambers grow significantly slower than in the control. (D,H) One-way ANOVA, $n=10$. (G,J) One-way ANOVA, $n=6$. * $P<0.03$, ** $P<0.002$, **** $P<0.0001$, Tukey's post-hoc analysis. n =number of egg chambers. All experiments were replicated at least times and data are mean \pm s.e.m.

e.g. Movie 2). These types of nurse cable growth defects were very rarely observed in the *MDD>* control (Fig. 5E). Interestingly, all of the follicle cables remaining in the *dia-dsRNA* knockdown egg chambers had a significantly reduced growth rate compared with *MDD>* (Fig. 5I,J). This suggests that the follicle cables are more sensitive to *Dia* reduction, consistent with the absence of *Ena* on the follicle side of the cortex.

Although these phenotypes are consistent with the hypothesis that *Dia* is important for the growth of all nurse cell cables, the partial knockdown prevented us from determining whether formins are absolutely required for cable growth. To address this, we added a formin inhibitor, SMIFH2 (Rizvi et al., 2009), to the medium at the start of imaging. We assessed cable length over time (Fig. 6A,C) and calculated the 'instantaneous growth rate' over the 90 min imaging period by calculating the derivative of the nurse cable length and averaging the derivatives before and after each timepoint (Fig. 6B). This allowed us to compare the growth rates over time. By 30–45 min after the addition of 200 μM inhibitor, cable growth rate was significantly reduced and, after 45 min, the growth rate was no longer significantly different from 0 $\mu\text{m}/\text{min}$ (Fig. 6A–C). At 100 μM SMIFH2, nurse cable growth rate did not slow significantly, but cable growth stopped completely after 75 min (Fig. 6A–C, e.g. Movie 3). Furthermore, when we simultaneously treated with 100 μM SMIFH2 and expressed *dia-dsRNA*, nurse cell cable growth decreased to zero immediately after treatment (Fig. 6D–F). These results strongly suggest that formins are necessary for nurse cable growth. Interestingly, with 100 μM inhibitor, the actin cables were contorted as they grew (Fig. 6G–I, Movie 3). In contrast to the dose-dependent effects of SMIFH2 on nurse cable growth, the formin inhibitor had a faster and stronger effect on follicle cables (Fig. 6J–L).

At both 100 μM and 200 μM , follicle cable growth stopped completely by 15–30 min after inhibitor addition.

Reduction of *Ena* decreases nurse cable density and growth rate, but does not disrupt follicle cable density or growth rate

Because *Ena* does not localize to the nurse cell cortex bordering the follicle cells, we predicted that *Ena* would play an important role in the growth of all cables except the follicle cables. To test this, we reduced *Ena* in the nurse cells by driving *ena-dsRNA* with a strong germline driver (*MTD>*). This resulted in a significant decrease, but not complete loss, of *Ena* protein (Fig. S2F–H). Consistent with our hypothesis, *Ena* reduction significantly decreased nurse cable density (Fig. 7A–C), with no effect on follicle cable density (Fig. 7D–F). All of the remaining nurse cables exhibited a significant growth rate reduction, but the follicle cable growth rate was unaffected (Fig. 7G,H).

Mislocalization of *Ena* creates a uniform cable growth rate and is associated with altered nuclear repositioning, nuclear blockage of ring canals and incomplete dumping

Our model predicts that the spatial asymmetry in cable growth rate plays an important role in nurse cell nuclei relocation (Fig. 3E), and our data support the idea that the selective cortical localization of *Ena* is necessary for that asymmetry. We therefore asked whether mislocalization of *Ena* to the nurse cell cortex adjacent to the follicle cells would increase the rate of follicle cable growth and create uniform fast growing cable arrays. We overexpressed *Ena* using a stock containing three copies of *ena-mCherry* driven by the Ubiquitin promoter (3x*Ena*-mCh). This resulted in the mislocalization of *Ena* to the nurse cell cortex adjacent to the follicle

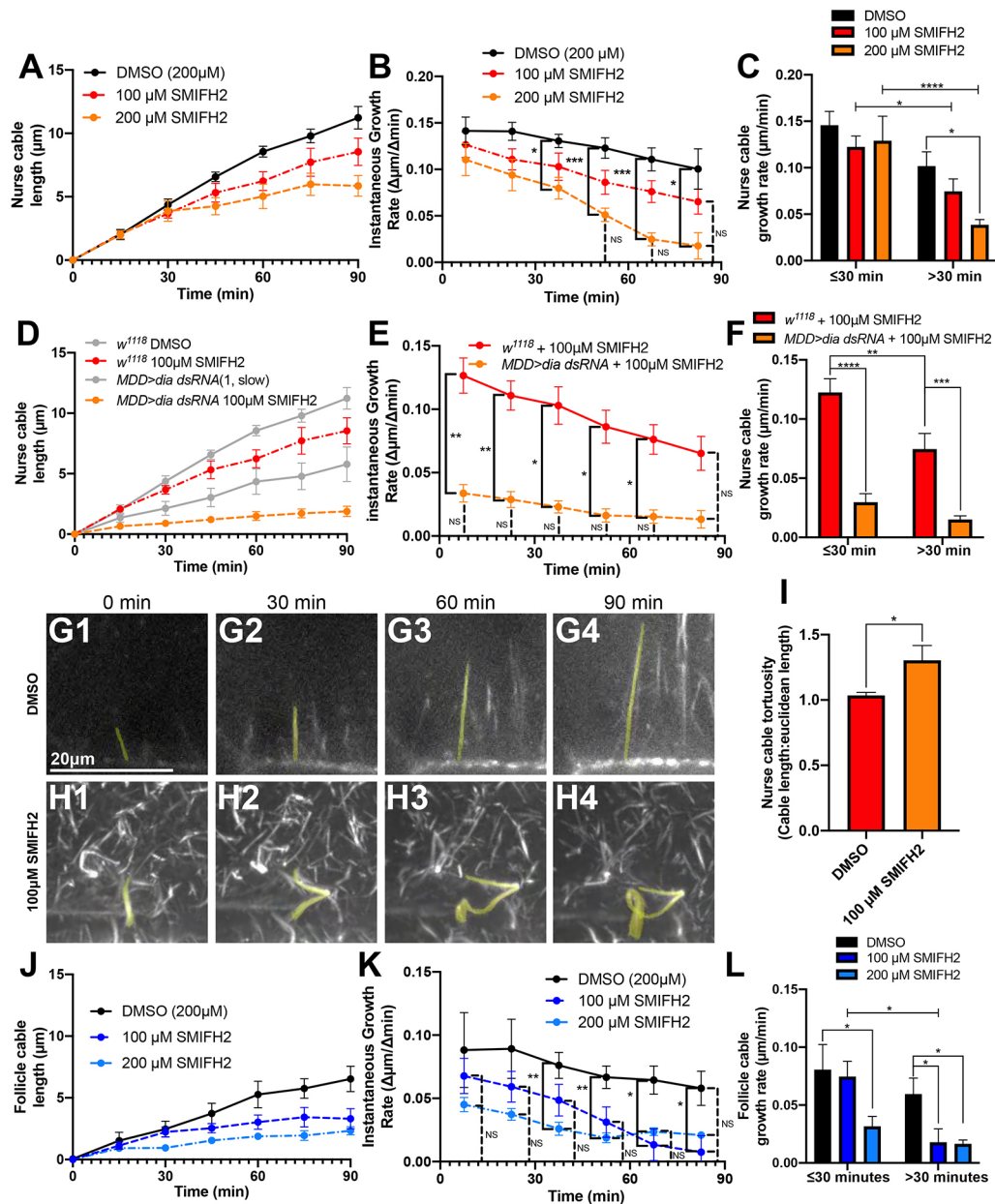


Fig. 6. Formins are required for nurse cable and follicle cable growth. (A) Nurse cable length over time after treatment with 100 μM SMIFH2, 200 μM SMIFH2 or DMSO. (B) Instantaneous growth rate calculated as the derivative of the curves in A. With the 200 μM treatment, the growth rate was not significantly different from 0 μm/min at the last three time points (NS). (C) Average growth rate in the first 30 min compared with the second 30 min after addition of DMSO or SMIFH2. (D) Nurse cable length over time for *w¹¹¹⁸* and *MDD>dia dsRNA* (1) egg chambers with and without 100 μM SMIFH2. Gray lines provide data from Fig. 5F for comparison. (E) Instantaneous growth rate, calculated as derivative of curves in C. Treatment of *dia-dsRNA* knockdown egg chambers with the formin inhibitor blocked nurse cable growth. (F) Average growth rate in the first 30 min compared with the second 30 min after addition of 100 μM SMIFH2. (G1-G4) Linear nurse cable growth in a DMSO-treated egg chamber. (H1-H4) Bent nurse cable growth in a wild-type egg chamber treated with 100 μM SMIFH2. (I) Quantification of nurse cable tortuosity. (J) Follicle cable length over time after treatment with 100 μM SMIFH2, 200 μM SMIFH2 or DMSO. (K) Instantaneous growth rate of follicle cables calculated as derivative of the curves in J. At both inhibitor concentrations, follicle cable growth was blocked immediately. (L) Average growth rate in the first 30 min compared with the second 30 min after addition of DMSO or SMIFH2. (B,C,E,F,K,L) Two-way ANOVA, $n=6$. (I) Two-tailed *t*-test, $n=6$. * $P<0.03$, ** $P<0.002$, *** $P<0.0002$, **** $P<0.0001$, Dunnett's multiple comparisons post-hoc analysis (B,D,I). n =number of egg chambers. All experiments were replicated at least three times and data are mean \pm s.e.m.

cells (Fig. 8A,B, arrowhead and insets). Consistent with our hypothesis, the follicle cable growth rate in 3xEna-mCh nurse cells significantly accelerated to match the rate of nurse cables in wild-type or 3xEna-mCh nurse cells (Fig. 8F,G). At the end of stage 10B, follicle cables and nurse cables in 3xEna-mCh nurse cells were of similar length (Fig. 8D,E arrowheads), whereas wild-type nurse cables (Fig. 8C, red arrowhead) tended to be much longer than

follicle cables (Fig. 8C, blue arrowhead). In addition to a faster growth rate, wild-type nurse cables are embedded in Ena-labelled pits (Fig. 4G-I) and preserved during fixation, suggesting that Ena might also confer these properties to the follicle cables. Contrary to this prediction, follicle cables were not preserved in 3xEna-mCh nurse cells and no Ena pits were observed (data not shown). Ena alone may not be sufficient for pit formation or pits may be

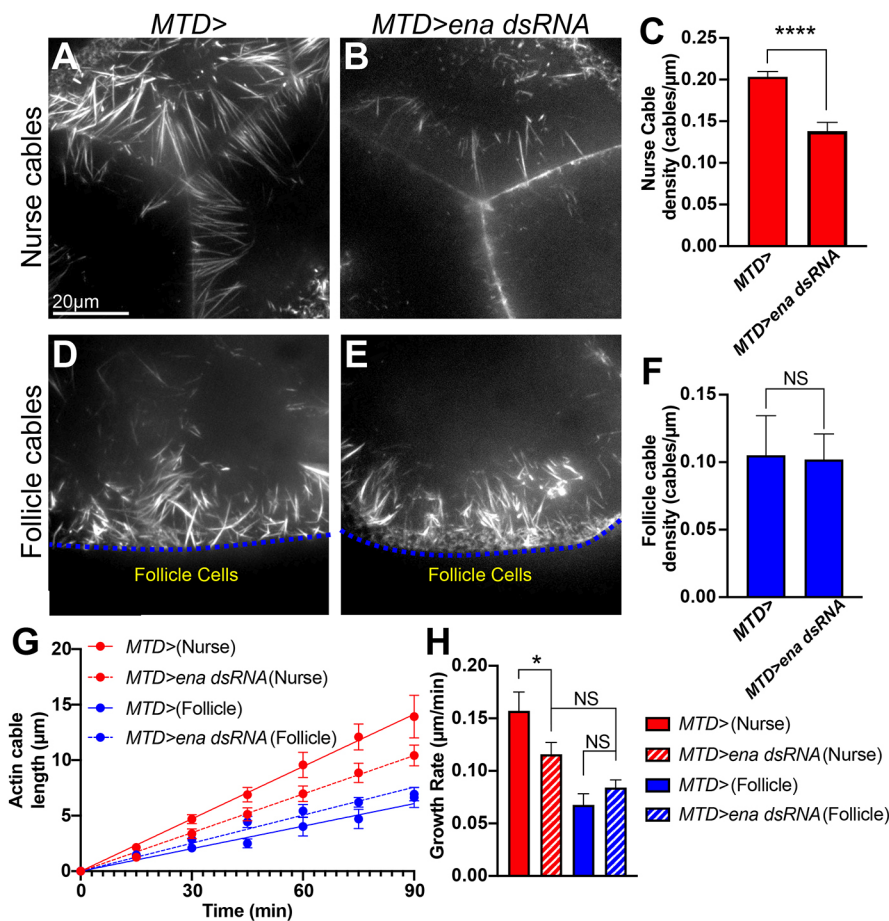


Fig. 7. Ena is required for normal nurse cable initiation and growth but is dispensable for follicle cables. Live images of nurse cables in control (A) and *ena* knockdown (B) egg chambers. (C) Nurse cable density is significantly lower in *ena* knockdown egg chambers. Live images of follicle cables in control (D) and *ena* knockdown (E) egg chambers. (F) Follicle cable density is not significantly different between control and *ena* knockdown. (G) Nurse and follicle cable length over time in control and *ena* knockdown egg chambers. (H) Nurse cables grow significantly slower when Ena is reduced, while follicle cable growth is unaffected. Two-tailed *t*-test, $n=10$ (C,F), $n=6$ (H). * $P<0.03$, **** $P<0.0001$. n =number of egg chambers. All experiments were replicated at least three times and data are mean \pm s.e.m.

unresolvable when Ena is overexpressed. Ena overexpression slightly, but not significantly, depressed the growth rate of wild-type nurse cables (Fig. 8F,G). This may suggest that mCherry-tagged Ena has partially reduced function. Regardless, the net result of Ena mislocalization was actin cable arrays with a uniform fast growth rate (Fig. 8G).

We next asked whether the uniform array would prevent the normal displacement of nurse cell nuclei before dumping. In some cases, one or two of the nurse cells can merge with the oocyte during stage 10B, followed by degeneration of their nuclei (Ali-Murthy et al., 2021). We counted nurse cell nuclei in fixed stage 11-12 *w¹¹¹⁸* and *3xEna-mCh* egg chambers ($n=19-22$), and in all cases we identified 15 nurse cell nuclei. If nurse cell fusion occurs, it appears rare and unlikely to impact our nuclear relocation analysis.

The position of a nurse cell in the 15 cell syncytium affects the position of the ring canals in that cell. To control for this variability, we characterized nuclear movement in nurse cells bordering the oocyte and the squamous follicular epithelium (Fig. 8H,H'). Based on ring canal position and our analysis of cable growth rate, we predicted that these nuclei would move toward the follicle cells (Fig. 8H'). Although the precise trajectory varied, all wild-type nuclei moved toward the nurse cell cortex at the follicle cell border, or toward the boundary between the anterior nurse cell and the adjacent follicle cells (Fig. 8I,K,L, black, e.g. Movie 4). When we equalized actin cable growth rate by mislocalizing Ena, the nuclei moved exclusively toward the anterior nurse cell and consequently toward the ring canal present at that boundary (Fig. 8J-L, magenta). Thus, we found that asymmetric cable growth in wild-type nurse cells is associated with a nuclear trajectory predicted to reduce

nuclear blockage of ring canals and promote dumping, while a uniform cable growth rate is associated with a nuclear trajectory predicted to increase the likelihood of nuclear blockage and inhibit dumping.

To assess dumping, we used the length of the oocyte and of the nurse cell cluster in stage 12 wild-type and *3xEna-mCh* egg chambers (Fig. 8M) to calculate the nurse cell to oocyte ratio. We found that this ratio was significantly increased in *3xEna-mCh* egg chambers (Fig. 8N), consistent with incomplete dumping. We observed a similar increase in the nurse cell to oocyte ratio in egg chambers where the actin cable arrays were altered through reduction of Ena or Dia (Fig. S3A,B). Those defects were weaker than with Ena overexpression, perhaps due to partial protein reduction (Fig. S2), to the specific effects on cable density and growth rate (Figs 5–7), or to other cytoskeletal effects. Complete loss of Ena produces a stronger dumping defect (Gates et al., 2009). Interestingly, the overall length of *3xEna-mCh* egg chambers was greater than wild type (Fig. 8O), perhaps due to effects of Ena overexpression earlier in oogenesis.

Our model predicts that the incomplete dumping is due to blockage of the ring canals by the nurse cell nuclei. Consistent with this, we found examples of nuclear extrusion through the ring canals in stage 12 *3xEna-mCh* egg chambers (Fig. 8Q1-Q2) reminiscent of *Singed/Fascin* and *Quail/Villin* mutants (Cant et al., 1994; Mahajan-Miklos and Cooley, 1994). We did not observe nuclear blockage in *w¹¹¹⁸* egg chambers (Fig. 8P1,P2). The reduced dumping in *3xEna-mCh* egg chambers could be solely due to nuclear relocation changes and ring canal blockage, but it is possible that Ena overexpression and mislocalization alter the nurse cell

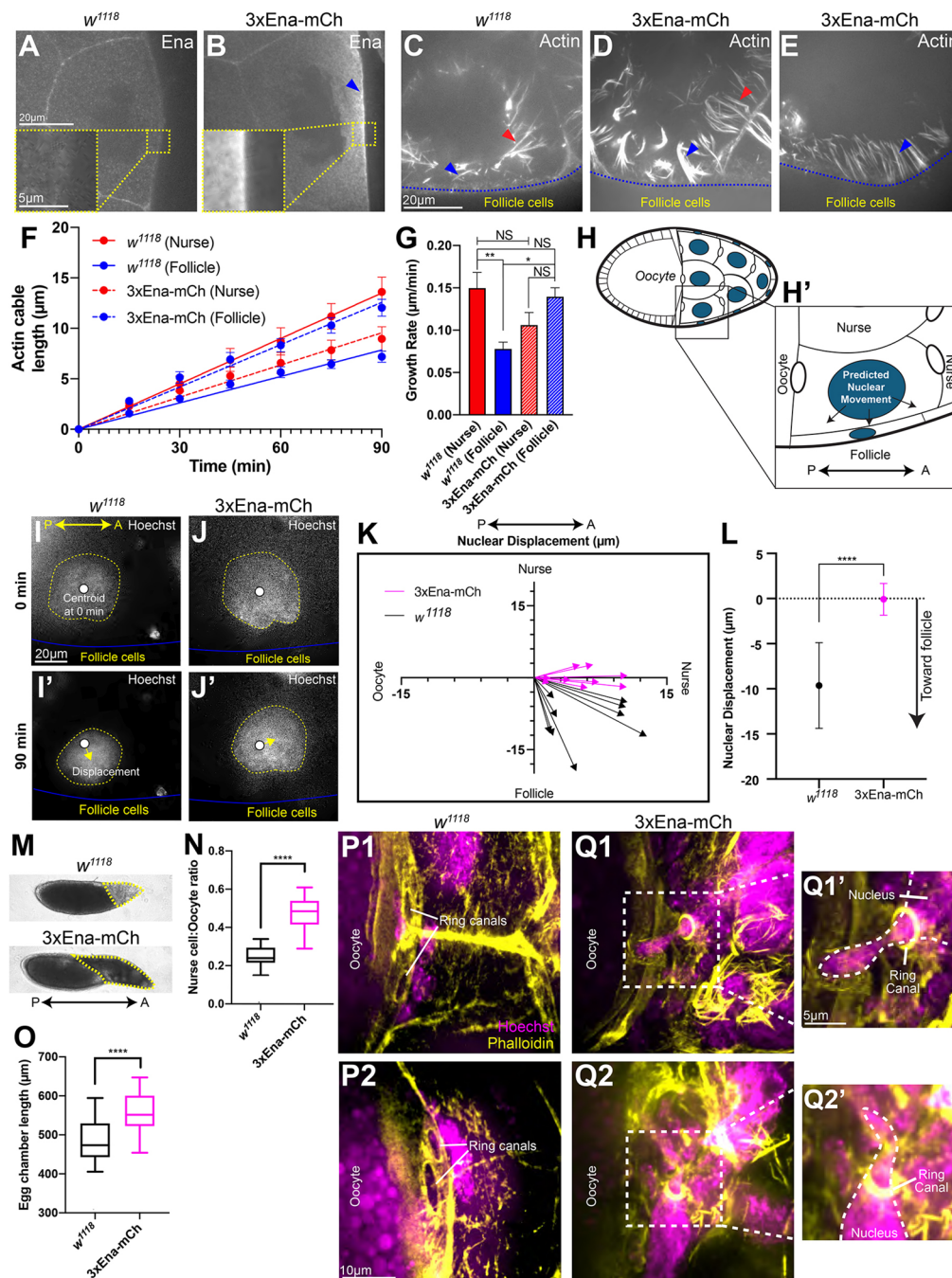


Fig. 8. Mislocalization of Ena is associated with uniform cable growth rate, defects in nuclear relocation, nuclear blockage of ring canals and incomplete dumping. (A,B) Expression of 3xEna-mCherry (mCh) results in mislocalization of Ena to the nurse cell cortex at the follicle cell border (blue arrowhead). (C-E) 5 μm z-projection of live, SiR-actin labelled egg chambers, showing nurse cables (red arrowheads) and follicle cables (blue arrowheads) in *w*¹¹¹⁸ (C) and 3xEna-mCh (D,E) egg chambers. (F) Nurse and follicle cable length over time in *w*¹¹¹⁸ and 3xEna-mCh egg chambers. (G) Nurse and follicle cable growth rate in *w*¹¹¹⁸ and 3xEna-mCh egg chambers. Follicle cable growth rate is significantly increased in 3xEna-mCh egg chambers. (H,H') Schematics of the position of the nurse cell that we selected to measure nuclear movement, depicting the predicted wild-type nuclear trajectory. (I,J) Live wild-type and 3xEna-mCh egg chambers showing that over 90 min the nucleus moves toward the follicular epithelium in a wild-type (I'), and toward the anterior nurse cell in a 3xEna-mCh (J') egg chamber. (K) Nuclear displacement trajectory and distance in *w*¹¹¹⁸ (black) and 3xEna-mCh (magenta) egg chambers over 90 min (*n*=10). (L) There is no significant nuclear displacement toward the follicular epithelium in 3xEna-mCh egg chambers (magenta). (M) Representative bright-field images showing nurse cells (yellow dashed lines) that do not complete dumping in 3xEna-mCh egg chambers. Nurse cell cluster: oocyte ratio (N) and total egg chamber length (O) for stage 12 *w*¹¹¹⁸ and 3xEna-mCh egg chambers. (P-Q2') Representative images of stage 12 *w*¹¹¹⁸ (P1,P2) and 3xEna-mCh (Q1,Q2) egg chambers showing examples of nuclear extrusion (Q1',Q2'). One-way ANOVA with Tukey's post-hoc analysis, *n*=6 (G). Two-tailed *t*-test, *n*=10 (L), *n*=21 (N,O). **P*<0.03, ***P*<0.002, *****P*<0.0001. *n*=number of egg chambers. All experiments were replicated at least three times and data are mean±s.e.m. with the exception of the box and whisker plots (N,O), where mean, min, max, and 25th and 75th percentiles are shown.

cortical contractility that contributes to reduced dumping. Likewise, Ena and Dia reduction may also affect cortical contractility or other cytoskeletal functions that contribute to incomplete dumping (Fig. S3A,B). Together, our results are consistent with the model that the asymmetric actin cable growth rate is necessary for proper nuclear relocation in nurse cells to enable the successful completion of cytoplasmic dumping and oogenesis.

DISCUSSION

Early work in fixed tissue suggested that the nurse cell actin cable arrays were static baskets, holding nurse cell nuclei in place while cytoplasm flowed past through the ring canals (Cant et al., 1994; Mahajan-Miklos and Cooley, 1994). Instead, live imaging revealed that the actin cable arrays actively contact and push the nuclei, rolling and wrapping them as the cables elongate (Huelsmann et al., 2013). We show that the actin cable arrays have regional growth rate asymmetry and demonstrate that loss of that asymmetry is associated with a loss of normal directional repositioning of nurse cell nuclei in a sample population, nuclear blockage of ring canals and incomplete dumping. Furthermore, we show that Dia and Ena are required to initiate and elongate the faster growing nurse cables, while Dia alone is necessary for the proper initiation and elongation of the slower growing follicle cables. Finally, our results suggest that selective localization of Ena is a key factor that establishes the actin cable growth rate asymmetry within each array.

The use of an asymmetric actin cable array to push and relocate nuclei is novel among the diversity of actin-based mechanisms for nuclear movement. Actomyosin contraction (Nakazawa and Kengaku, 2020; Sakamoto et al., 2020) and actin flows (Zhu et al., 2018) move nuclei in migrating cultured cells and neurons. Active diffusion of actin-coated vesicles driven by myosin Vb generates a pressure gradient and propulsive force to move the mouse oocyte nucleus (Almonacid et al., 2015). Actin cables are used in other contexts but, in those contexts, nuclei are coupled to actin cables used as tracks for nuclear transport (Folker et al., 2011; Luxton et al., 2010, 2011). The fish retinal neuroepithelium uses a different type of formin-dependent actin network to push nuclei apically, and cortex-anchored and bundled actin modulated by myosin may generate the pushing force (Yanakiya et al., 2019).

Our data suggest the nurse cell actin cable arrays push and reposition the nuclei due to the asymmetry in cable growth rates: the faster growing nurse and oocyte cables make first contact with the nucleus and begin to push it towards the slower growing cables on the follicle cell side of the nurse cell cortex (Fig. 3E). This is consistent with the overall trajectory of the nuclei toward the follicular epithelium and away from the ring canals in our sample nurse cell (Fig. 8I-L). Because oocyte cable and nurse cable dynamics are largely indistinguishable (Figs 2 and 3), it was surprising that the wild-type trajectory was typically away from the oocyte (Fig. 8K).

When we equalized cable growth rate through mislocalization of Ena, the nuclei embarked on a distinct trajectory toward the neighboring anterior nurse cell and the site of a ring canal connecting them (Fig. 8J-L). We were surprised that the nuclei moved at all – if the actin cable arrays were uniform in all features, the nuclei might be trapped by equivalent forces exerted on all sides. Stochastic differences in the ‘uniform’ cable arrays would likely result in random nuclear movement, not the directional movement we observed (Fig. 8K). This suggests that the apparently uniform cable arrays harbor unidentified asymmetries contributing to the directional, although misguided, nuclear movement. Such

unidentified asymmetries may also contribute to nuclear movement away from the oocyte under both conditions. In our quantification of nuclear movement trajectory and distance (Fig. 8K,L), we did not follow the specific paths that the nuclei take. Tracking the nuclei during movement in the future may provide new insights into how the actin cables accomplish repositioning.

The nurse cell actin cables share structural similarity with Listeria tails containing crosslinked actin filament bundles (Jasmin et al., 2013), and with filopodia that typically contain a single bundle of 10–30 unidirectional linear actin filaments extending from a few to 100 μm (Leijnse et al., 2015). Cables can be viewed simply as inverted filopodia where the actin bundles extend into the cytoplasm rather than away from the cell body. Despite this difference in orientation, cables and filopodia both use formins and Ena/VASP proteins to assemble filaments bundled by Fascin and Villin (Gates et al., 2009; Huelsmann and Brown, 2014; Leijnse et al., 2015; Figs 5–7). In filopodia, Ena localizes to a well described ‘tip complex’ at the distal end of the filopodium that elongates away from the cell body. Ena similarly localizes to the base of nurse cables and oocyte cables, the site of filament assembly (Guild et al., 1997), that project outward 1–2 μm in cable pits that protrude into neighboring nurse cells (Gates et al., 2009; Guild et al., 1997; Fig. 4G-I). We found that Dia also localizes to these pits along the shaft and with Ena in the tip (Fig. 4G-I). Similar to cable pits, endogenous Ena and Dia are sometimes associated with the same filopodium with Ena at the tip and Dia in the shaft (Bilancia et al., 2014).

The functional relationship between formins and Ena/VASP in filopodia is complex. Independently, they create filopodia and other projections with distinct morphological, dynamic and functional properties (Barzik et al., 2014; Bilancia et al., 2014; Homem and Peifer, 2008, 2009; Nowotarski et al., 2014). For example, Bilancia et al. (2014) showed that in *Drosophila* D16 cultured cells, Ena overexpressed alone promoted filopodia that exhibited dynamic changes in number, length and lifetime. In contrast, Dia overexpressed alone promoted long and stable filopodia. These *in vivo* effects may be explained in part by their different *in vitro* activities. Because Ena is slower and less processive than Dia, other actin modifiers may have the opportunity to alter the developing filopodia. When Dia and Ena were co-overexpressed, the cells produced fewer and shorter filopodia, suggesting that Ena inhibits Dia. Consistent with that, the Ena EVH1 domain binds Dia and inhibits its nucleation activity *in vitro*, and when Dia and Ena colocalized in the tip complex, the majority of filopodia retracted, folded back or stalled.

Our data suggest that Dia and Ena collaborate to assemble nurse cables and oocyte cables, but the functional consequence of the interaction appears different from that observed in filopodia. First, endogenous Dia consistently localizes with Ena in the cable pit (Fig. 4G,I), and can colocalize with Ena in the tip (Fig. 4H,I), suggesting that colocalization does not terminate cable growth. Furthermore, our functional data are most consistent with a Dia-Ena collaboration in both cable initiation and elongation, as reduction/inhibition of either protein significantly reduced cable number and slowed or halted nurse cable growth (Figs 5–7). Interestingly, the nurse and oocyte cables are also faster growing than the follicle cables where Dia functions without Ena (Figs 5–7). This suggests that the Dia-Ena collaboration may accelerate filament assembly, or that other factors modulate cable growth rate of one or both cable types.

Our model proposes that the selective localization of Ena is a key factor generating the asymmetric actin cable array. Adherens junctions between nurse cells, and between the nurse cells and the

oocyte, is one way in which this cortical region differs from that adjacent to the follicle cells. Another potential regulator of Ena localization is prostaglandin signaling, which contributes to proper Ena localization during stage 10B (Spracklen et al., 2014b) and is required for nurse cell dumping (Tootle and Spradling, 2008). Lamellipodin (Lpn, *Drosophila* Pico) is important for the localization of Ena to lamellipodia in mammalian cells (Carmona et al., 2016; Cheng and Mullins, 2020; Hansen and Mullins, 2015; Michael et al., 2010), and also contributes to nurse cell dumping (Spracklen et al., 2019). Loss of Abelson (Abl), a tyrosine kinase targeting Ena, results in a dumping defect, premature cable assembly and some abnormal Ena localization (Gates et al., 2009). The selective cortical localization of Ena in epithelia and other cell types is also thought to influence protrusive activity and interactions with Dia (Bilancia et al., 2014; Gates et al., 2007; Homem and Peifer, 2009; Nowotarski et al., 2014). Thus, tight control of the cortical localization of Ena may be a general mechanism regulating the actin filament assembly that controls a wide variety of processes from cell migration to morphogenesis and nuclear positioning.

MATERIALS AND METHODS

Flies

The following stocks were used: w^{1118} (a wild-type control strain), $y^1 w$; $P\{matalpha4-GAL-VP16\}67$; $P\{matalpha4-GAL-VP16\}15$ (*MDD-GAL4*; Bloomington, 80361), $P\{w[+mC]=otu-GAL4::VP16.R\}1$, w ; $P\{w[+mC]=GAL4-nos.NGT\}40$; $P\{w[+mC]=GAL4::VP16-nos.UTR\}CG6325[MVD1]$ (*MTD-GAL4*; Bloomington, 31777), w ; $P\{w[+mC]=UAS-p-F-Tractin.tdTomato\}15A/SM6b$ (*UAS-Fractin.tdTomato*; Bloomington, 58989), w ; $P\{w[+mC]=UAS-Lifeact.GFP.W\}3$ (*UAS-LifeAct-GFP*; Bloomington, 57326), $y^1 sc v^1 sev^{21}$; $P\{y[+t7.7]v[+t1.8]=TRiP.HMS00308\}attP2$ (*UAS-dia-dsRNA*(1); Bloomington, 33424), $y^1 sc v^1 sev^{21}$; $P\{y[+t7.7]v[+t1.8]=TRiP.GL00408\}attP40/CyO$ (*UAS-dia-dsRNA*(2), Bloomington, 35479), $y^1 sc v^1 sev^{21}$; $P\{y[+t7.7]v[+t1.8]=TRiP.HMS01953\}attP2$ (*UAS-ena-dsRNA*; Bloomington, 39034) and w ; $P\{w[+mC]=Ubi-mCherry.ena.D\}2/CyO$; $P\{w[+mC]=Ubi-mCherry.ena.D\}3$ (*Ubi-ena-mCherry*; Bloomington, 58731). FlyBase was used for gene information (Larkin et al., 2021).

Imaging

24 h before all experiments, flies were fed wet yeast paste to promote egg production. For live-imaging experiments, stage 10B egg chambers were isolated as described previously (Spracklen and Tootle, 2013). Egg chambers were imaged in live imaging media consisting of Schneider's media with 20% fetal bovine serum (FBS), 5 μ g/ml insulin, 2 mg/ml trehalose, 5 μ M methoprene, 1 μ g/ml 20-hydroxyecdysone and 50 ng/ml adenine deaminase in Concanavalin A-coated glass-bottom petri dishes (Azer Scientific ES56291). At the start of imaging, egg chambers were labeled with the nuclear stain Hoechst (1:1000, Invitrogen, 33342) and/or 1:1000 SiR-actin (Spirochrome, CY-SC001, Stein am Rhein, Switzerland). For w^{1118} actin cable characterization experiments (Figs 2,3), we used an Andor Revolution XD spinning disk confocal microscope. All other images were acquired with a Prime95B CMOS camera (Photometrics) on a Zeiss Axiovert 200 M microscope with a X-Light V2 spinning disc scan head (Crest Optics). Fluorophores were excited with a Celesta Light Engine (Lumencor). For live imaging, stacks (z-step 0.5 μ m) were taken every 15 min for 90 min. Because the cable growth rate was relatively slow, a 15 min interval gave us sufficient temporal resolution and minimized potential tissue damage due to laser exposure. For formin inhibition experiments, SMIFH2 (Sigma-Aldrich, S4826) or DMSO was added directly to the imaging media at the beginning of the imaging period. Ovaries were fixed for 20 min in 4% paraformaldehyde diluted in phosphate buffered saline (PBS) from an 8% stock (EMS, 157-8) and blocked for 1 h in PBS plus 0.2% Triton X-100 and 4% normal goat serum (NGS). Antibody/label incubations were in PBS plus 0.1% Triton X-100 and 1% NGS using 1:500 Alexa488-Phalloidin (Thermo Fisher Scientific, A12379), 1:1000

Hoechst (Invitrogen, 33342) and the following antibodies: 1:1000 mouse anti-Ena (DSHB, 5G2) and 1:1000 rabbit anti-Dia (a gift from the Wasserman lab, University of California San Diego, USA).

Quantification of actin cable properties and growth dynamics

To quantify cable initiation and density, where it is crucial to detect cables in early stage 10B, verapamil (1:1000) was added to the media to increase the rate of SiR-actin labeling. For all experiments, n refers to the number of egg chambers. Where relevant, five cables per egg chamber were analyzed. For initiation measurements, the number of cables less than 3 μ m long was measured at each timepoint along two or three spans of membrane per egg chamber totaling a distance of 120–240 μ m for nurse borders, 70–100 μ m for oocyte borders and 60–140 μ m for follicle borders. The predicted density was measured as the cumulative sum of all new cables on and before each timepoint. For density measurements, the total number of actin cables was measured over five spans of nurse cell borders totaling 150–240 μ m in length, two to five spans of oocyte borders totaling 60–220 μ m in length, and two or three spans of follicle borders totaling 70–170 μ m in length. For cable growth rates, the length of five actin cables in each of six egg chambers was tracked over the imaging period and linear regressions were taken to determine the growth rate of each cable. Length was measured by calculating the Euclidian distance between the cable base at the cortex, and the distal tip of each actin cable. Because z-resolution is lower than x/y resolution, we selected actin cables that were largely in the same z plane during the imaging period (e.g. Movie 1). To measure time of dumping or nuclear movement, we measured the length of 10 nurse cables from egg chambers at the beginning of dumping (marked by decreasing nurse cell size) or from egg chambers at the beginning of nuclear movement, then we calculated the time of dumping or nuclear movement by dividing the average cable length of each egg chamber by the average nurse cell growth rate. To determine the percentage of cables that contact the nucleus, we assessed nuclear contact of 10–20 randomly chosen cables from two or three nurse cells per egg chamber. For tortuosity measurements, we measured the actual length of 10 cables and divided by the Euclidean distance of each cable (linear distance between the barbed and pointed ends). When measuring growth rate for experiments where it is not crucial to include the beginning of stage 10B, we subtracted the length of each cable by the length of the cable at t0; this allowed for uniform growth curves with the length of each curve starting at 0 μ m. Instantaneous growth rate was calculated using the derivative tool in Prism 8 and smoothing the resulting curve by averaging each value with its neighboring values.

Quantification of nuclear displacement

All nuclear displacement measurements were carried out in nurse cells directly adjacent to the oocyte, and images were rotated or flipped so the oocyte was to the left of the nurse cell and the follicle was to the bottom. To take movement of the egg chamber into account, we determined cell-normalized nuclear location by subtracting the centroid coordinates of the nucleus by the centroid coordinates of the nurse cell at 0 min and 90 min. For graphical representation, we generated vectors from the centroid at 0 min to the centroid at 90 min and transformed each vector to the origin of the graph. The displacement towards the follicle is the displacement along the y-axis of each vector. We followed nuclei for 90 min from the start of imaging, selecting for analysis only egg chambers at the developmental stage where the nucleus was expected to move, which we identified as the point where all cables begin to contact the nucleus (Fig. 3D).

Quantification of fluorescence intensity

We calculated Dia and Ena intensity in fixed egg chambers by measuring average intensity along five segments (~5 μ m long) of nurse border, follicle border or cytoplasm in each of six egg chambers. Dia and Ena colocalized pixels in Fig. 4H were highlighted using the 'colocalization' plug-in in ImageJ (Fiji v.1.53q) with a threshold of 150 for Dia and 255 for Ena.

Image analysis and statistics

We performed all measurements using ImageJ (version 2.0.0). All analysis and graphs were generated with Prism 8 (Graphpad), and figures were

prepared using Adobe Illustrator. Tests for normal distributions and outliers were conducted with Prism 8.

Acknowledgements

Thank you to Haibing Teng and the Molecular Biosensor and Imaging Center (MBIC) at Carnegie Mellon University for providing us with some imaging resources. The anti-Dia antibody was a gift from S. Wasserman (UCSD). Many thanks to O. Molinar-Inglis for initiating this work and to C. A. Ettensohn for valuable comments on the manuscript. Stocks obtained from the Bloomington *Drosophila* Stock Center (NIH P40OD018537) were used in this study.

Competing interests

The authors declare no competing or financial interests.

Author contributions

Conceptualization: G.L., B.M.M.; Methodology: G.L., B.M.M.; Formal analysis: G.L.; Investigation: G.L., W.-C.C.; Writing - original draft: G.L., B.M.M.; Writing - review & editing: G.L., B.M.M.; Supervision: B.M.M.; Funding acquisition: B.M.M.

Funding

This work was funded by a grant to B.M.M. from the National Institutes of Health (R01-GM120378). Deposited in PMC for release after 12 months.

References

- Ali-Murthy, Z., Fetter, R. D., Wang, W., Yang, B., Royer, L. A. and Kornberg, T. B. (2021). Elimination of nurse cell nuclei that shuttle into the oocytes during oogenesis. *J. Cell Biol.* **220**, e202012101. doi:10.1083/jcb.202012101
- Almonacid, M., Ahmed, W. W., Bussonnier, M., Mailly, P., Betz, T., Voituriez, R., Gov, N. R. and Verhac, M.-H. (2015). Active diffusion positions the nucleus in mouse oocytes. *Nat. Cell Biol.* **17**, 470-479. doi:10.1038/ncb3131
- Azevedo, M. and Baylies, M. K. (2020). Getting into position: nuclear movement in muscle cells. *Trends Cell Biol.* **30**, 303-316. doi:10.1016/j.tcb.2020.01.002
- Barzik, M., McClain, L. M., Gupton, S. L. and Gertler, F. B. (2014). Ena/VASP regulates mDia2-initiated filopodial length, dynamics, and function. *Mol. Biol. Cell* **25**, 2604-2619. doi:10.1091/mbc.e14-02-0712
- Bilancia, C. G., Winkelman, J. D., Tsygankov, D., Nowotarski, S. H., Sees, J. A., Comber, K., Evans, I., Lakhani, V., Wood, W., Elston, T. C. et al. (2014). Enabled negatively regulates diaphanous-driven actin dynamics in vitro and in vivo. *Dev. Cell* **28**, 394-408. doi:10.1016/j.devcel.2014.01.015
- Cant, K., Knowles, B. A., Moosker, M. S. and Cooley, L. (1994). *Drosophila* singed, a fascin homolog, is required for actin bundle formation during oogenesis and bristle extension. *J. Cell Biol.* **125**, 369-380. doi:10.1083/jcb.125.2.369
- Carmona, G., Perera, U., Gillett, C., Naba, A., Law, A. L., Sharma, V. P., Wang, J., Wyckoff, J., Balsamo, M., Mosis, F. et al. (2016). Lamellipodin promotes invasive 3D cancer cell migration via regulated interactions with Ena/VASP and SCAR/WAVE. *Oncogene* **35**, 5155-5169. doi:10.1038/ncr.2016.47
- Cheng, K. W. and Mullins, R. D. (2020). Initiation and disassembly of filopodia tip complexes containing VASP and lamellipodin. *Mol. Biol. Cell* **31**, 2021-2034. doi:10.1091/mbc.E20-04-0270
- Folker, E. S., Östlund, C., Luxton, G. W., Worman, H. J. and Gundersen, G. G. (2011). Lamin A variants that cause striated muscle disease are defective in anchoring transmembrane actin-associated nuclear lines for nuclear movement. *Proc. Natl. Acad. Sci. USA* **108**, 131-136. doi:10.1073/pnas.1000824108
- Gates, J., Mahaffey, J. P., Rogers, S. L., Emerson, M., Rogers, E. M., Sottile, S. L., Van Vactor, D., Gertler, F. B. and Peifer, M. (2007). Enabled plays key roles in embryonic epithelial morphogenesis in *Drosophila*. *Development* **134**, 2027-2039. doi:10.1242/dev.02849
- Gates, J., Nowotarski, S. H., Yin, H., Mahaffey, J. P., Bridges, T., Herrera, C., Homem, C. C., Janody, F., Montell, D. J. and Peifer, M. (2009). Enabled and Capping protein play important roles in shaping cell behavior during *Drosophila* oogenesis. *Dev. Biol.* **333**, 90-107. doi:10.1016/j.ydbio.2009.06.030
- Gönczy, P., Pichler, S., Kirkham, M. and Hyman, A. A. (1999). Cytoplasmic dynein is required for distinct aspects of MTOC positioning, including centrosome separation, in the one cell stage *Caenorhabditis elegans* embryo. *J. Cell Biol.* **147**, 135-150. doi:10.1083/jcb.147.1.135
- Guild, G. M., Connelly, P. S., Shaw, M. K. and Tilney, L. G. (1997). Actin filament cables in *Drosophila* nurse cells are composed of modules that slide passively past one another during dumping. *J. Cell Biol.* **138**, 783-797. doi:10.1083/jcb.138.4.783
- Gundersen, G. G. and Worman, H. J. (2013). Nuclear positioning. *Cell* **152**, 1376-1389. doi:10.1016/j.cell.2013.02.031
- Hansen, S. D. and Mullins, R. D. (2015). Lamellipodin promotes actin assembly by clustering Ena/VASP proteins and tethering them to actin filaments. *Elife* **4**, 1-29. doi:10.7554/eLife.06585
- Homem, C. C. and Peifer, M. (2008). Diaphanous regulates myosin and adherens junctions to control cell contractility and protrusive behavior during morphogenesis. *Development* **135**, 1005-1018. doi:10.1242/dev.016337
- Homem, C. C. and Peifer, M. (2009). Exploring the roles of diaphanous and enabled activity in shaping the balance between filopodia and lamellipodia. *Mol. Biol. Cell* **20**, 5138-5155. doi:10.1091/mbc.e09-02-0144
- Huelsmann, S. and Brown, N. H. (2014). Nuclear positioning by actin cables and perinuclear actin: Special and general? *Nucleus* **5**, 219-223. doi:10.4161/nucl.29405
- Huelsmann, S., Ylännä, J. and Brown, N. (2013). Filopodia-like actin cables position nuclei in association with perinuclear actin in *Drosophila* nurse cells. *Dev. Cell* **26**, 604-615. doi:10.1016/j.devcel.2013.08.014
- Jasnin, M., Asano, S., Gouin, E., Hegerl, R., Plitzko, J. M., Villa, E., Cossart, P. and Baumeister, W. (2013). Three-dimensional architecture of actin filaments in *Listeria monocytogenes* comet tails. *Proc. Natl. Acad. Sci. USA* **110**, 20521-20526. doi:10.1073/pnas.1320155110
- King, R. C. (1971). Ovarian development in *Drosophila melanogaster*. *Q. Rev. Biol.* **46**, 79. doi:10.1086/406775
- Larkin, A., Marygold, S. J., Antonazzo, G., Attrill, H., dos Santos, G., Garapati, P. V., Goodman, J. L., Gramates, L. S., Millburn, G., Strelets, V. B. et al.; the Flybase Consortium. (2021). Flybase: updates to the *Drosophila melanogaster* knowledge base. *Nucl. Acids Res.* **49**, D899-D907. doi:10.1093/nar/gkaa1026
- Leijnse, N., Oddershede, L. B. and Bendix, P. M. (2015). An updated look at actin dynamics in filopodia. *Cytoskeleton* **72**, 71-79. doi:10.1002/cm.21216
- Luxton, G. W., Gomes, E. R., Folker, E. S., Vintinner, E. and Gundersen, G. G. (2010). Linear arrays of nuclear envelope proteins harness retrograde actin flow for nuclear movement. *Science* **329**, 956-959. doi:10.1126/science.1189072
- Luxton, G. W., Gomes, E. R., Folker, E. S., Worman, H. J. and Gundersen, G. G. (2011). TAN lines: a novel nuclear envelope structure involved in nuclear positioning. *Nucleus* **2**, 173-181. doi:10.4161/nucl.2.3.16243
- Mahajan-Miklos, S. and Cooley, L. (1994). The villin-like protein encoded by the *Drosophila* quail gene is required for actin bundle assembly during oogenesis. *Cell* **78**, 291-301. doi:10.1016/0092-8674(94)90298-4
- Michael, M., Vehlow, A., Navarro, C. and Krause, M. (2010). c-Abl, Lamellipodin, and Ena/VASP proteins cooperate in dorsal ruffling of fibroblasts and axonal morphogenesis. *Curr. Biol.* **20**, 783-791. doi:10.1016/j.cub.2010.03.048
- Nakazawa, N. and Kengaku, M. (2020). Mechanical regulation of nuclear translocation in migratory neurons. *Front. Cell Dev. Biol.* **8**, 150. doi:10.3389/fcell.2020.00150
- Nowotarski, S. H., McKeon, N., Moser, R. J. and Peifer, M. (2014). The actin regulators enabled and diaphanous direct distinct protrusive behaviors in different tissues during *Drosophila* development. *Mol. Biol. Cell* **25**, 3147-3165. doi:10.1091/mbc.e14-05-0951
- Rizvi, S. A., Neidt, E. M., Cui, J., Feiger, Z., Skau, C. T., Gardel, M. L., Kozmin, S. A. and Kovar, D. R. (2009). Identification and characterization of a small molecule inhibitor of formin-mediated actin assembly. *Chem. Biol.* **16**, 1158-1168. doi:10.1016/j.chembiol.2009.10.006
- Sakamoto, R., Tanabe, M., Hiraiwa, T., Suzuki, K., Ishiwata, S., Maeda, Y. T. and Miyazaki, M. (2020). Tug-of-war between actomyosin-driven antagonistic forces determines the positioning symmetry in cell-sized confinement. *Nat. Commun.* **11**, 3063. doi:10.1038/s41467-020-16677-9
- Spracklen, A. J. and Tootle, T. L. (2013). The utility of stage-specific mid-to-late *Drosophila* follicle isolation. *J. Vis. Exp.* **82**, e50493. doi:10.3791/50493
- Spracklen, A. J., Fagan, T. N., Lovander, K. E. and Tootle, T. L. (2014a). The pros and cons of common actin labeling tools for visualizing actin dynamics during *Drosophila* oogenesis. *Dev. Biol.* **393**, 209-226. doi:10.1016/j.ydbio.2014.06.022
- Spracklen, A. J., Kelsch, D. J., Chen, X., Spracklen, C. N. and Tootle, T. L. (2014b). Prostaglandins temporally regulate cytoplasmic actin bundle formation during *Drosophila* oogenesis. *Mol. Biol. Cell* **25**, 397-411. doi:10.1091/mbc.e13-07-0366
- Spracklen, A. J., Lamb, M. C., Groen, C. M. and Tootle, T. L. (2019). Pharmacogenetic screen to uncover actin regulators targeted by prostaglandins during *Drosophila* oogenesis. *G3: Genes Genomes Genet.* **9**, 3555-3565. doi:10.1534/g3.119.400704
- Tissot, N., Lepesant, J. A., Bernard, F., Legent, K., Bosveld, F., Martin, C., Faklaris, O., Bellaïche, Y., Coppey, M. and Guichet, A. (2017). Distinct molecular cues ensure a robust microtubule-dependent nuclear positioning in the *Drosophila* oocyte. *Nat. Commun.* **8**, 15168. doi:10.1038/ncomms15168
- Tootle, T. L. and Spradling, A. C. (2008). *Drosophila* Pxt: a cyclooxygenase-like facilitator of follicle maturation. *Development* **135**, 839-847. doi:10.1242/dev.017590
- Vasicova, P., Rinnerthaler, M., Haskova, D., Novakova, L., Malcova, I., Breitenbach, M. and Hasek, J. (2016). Formaldehyde fixation is detrimental to actin cables in glucose-depleted *S. cerevisiae* cells. *Microb. Cell* **3**, 206-214. doi:10.15698/mic2016.05.499
- Yanakiya, I., Erzberger, A., Matejčić, M., Modes, C. D. and Norden, C. (2019). Cell and tissue morphology determine actin-dependent nuclear migration mechanisms in neuroepithelia. *J. Cell Biol.* **218**, 3272-3289. doi:10.1083/jcb.201901077
- Zhu, R., Liu, C. and Gundersen, G. G. (2018). Nuclear positioning in migrating fibroblasts. *Semin. Cell Dev. Biol.* **82**, 41-50. doi:10.1016/j.semcdb.2017.11.006

Figure S1

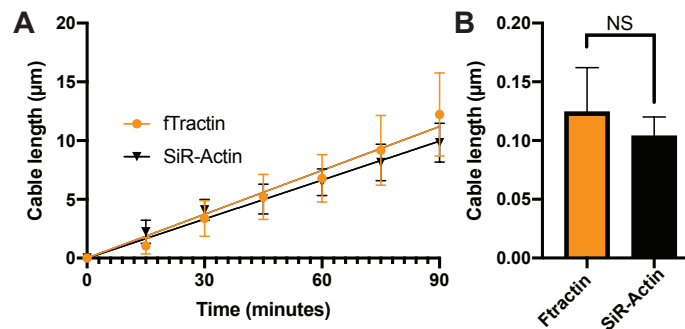


Fig. S1. (A,B) Nurse cable growth rate is indistinguishable in *fTractin-tdTomato* expressing nurse cells and *w¹¹¹⁸* (wild type) nurse cells labelled with SiR-Actin. Two-tailed t-test, *n*=6.

Figure S2

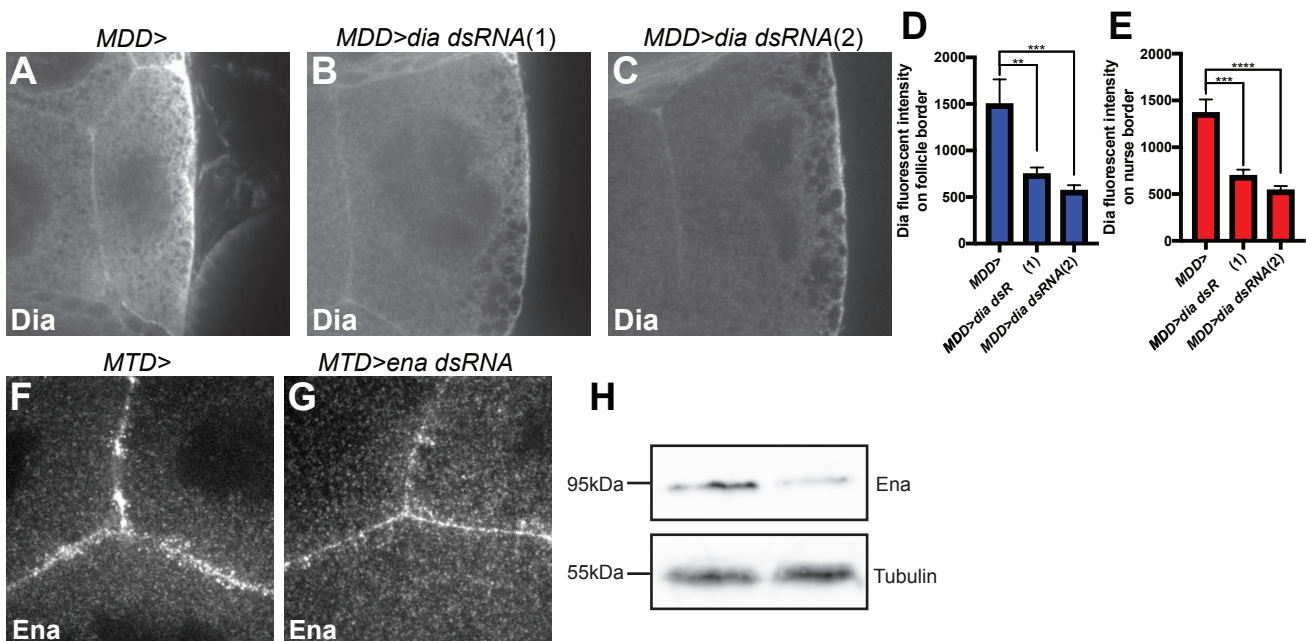


Fig.S2. (A-C) Dia immunostaining in fixed control (A) and *dia* knockdown (B-C) egg chambers. (D,E) Dia fluorescent intensity at the follicle border (D) and nurse border (E). (F,G) Ena immunostaining in fixed control (F), and *ena* knockdown (G) egg chambers. (H) Immunoblot of Ena and tubulin (loading control) in control and *ena* knockdown ovaries. One-way ANOVA Tukey's post-hoc analysis, ***p*<0.002, ****p*<0.0002, *****p*<0.0001.

Figure S3

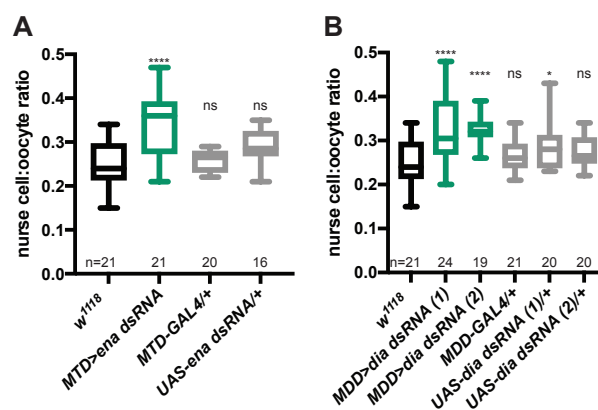
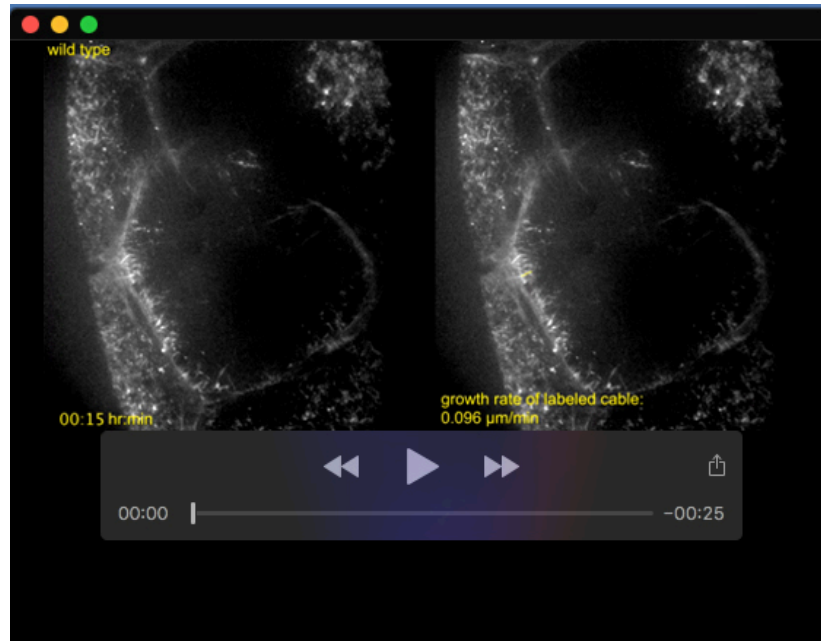
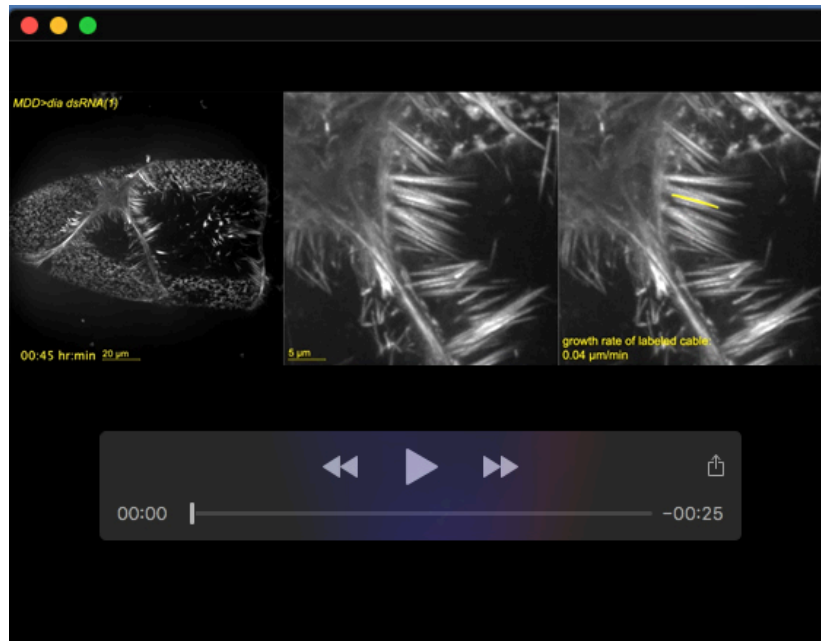


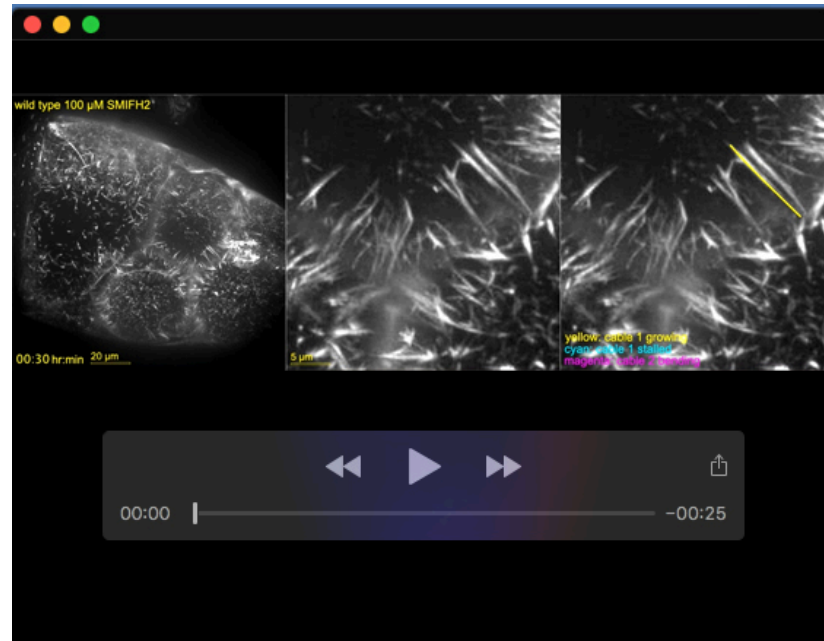
Fig. S3. *ena* (A) and *dia* (B) knockdown egg chambers have a significantly increased nurse cell to oocyte ratio consistent with incomplete dumping. n as indicated. One-way ANOVA Tukey's post-hoc analysis, * $p < 0.05$, ** $p < 0.01$, **** $p < 0.0001$.



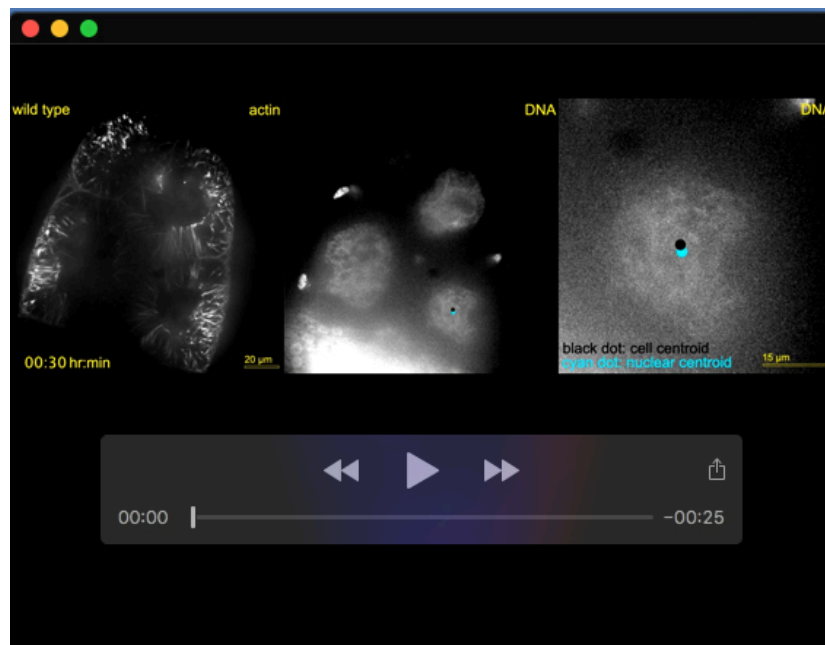
Movie 1. 120 min of actin cable growth in a SiR-Actin labeled wild type (*w¹¹¹⁸*) stage 10B egg chamber. Images were taken every 15 min. The labeled cable is growing at approximately 0.096 $\mu\text{m}/\text{min}$, typical for wild type nurse cables (Fig. 3B). Cable length was assessed by measuring the Euclidian distance between the cortex and the distal tip of an actin cable. Each frame is a maximum projection of 15 optical slices at 0.5 μm step size.



Movie 2. 90 min of actin cable growth in a SiR-Actin labeled *MDD>dia dsRNA(1)* stage 10B egg chamber. Images were taken every 15 min. The labeled cable is growing at approximately 0.04 $\mu\text{m}/\text{min}$, typical of the slow growing nurse cables in this genotype (Fig. 5G). Cable length was assessed by measuring the Euclidian distance between the cortex and the distal tip of an actin cable. Each frame is a maximum projection of 16 optical slices at 0.5 μm step size.



Movie 3. 75 min of actin cable growth in a SiR-Actin labeled wild type (w^{1118}) stage 10B egg chamber treated with 100 μM of the formin inhibitor SMIFH2. Images were taken every 15 min. This video illustrates two significant differences we observed with inhibitor treatment of wild type egg chambers. For the first 30-35 min in the inhibitor, cable growth proceeds as normal (yellow), but by approximately 45 min the cables stop growing (cyan; Fig. 6A-C). In addition, some cables bent as they grew (magenta; Fig. 6G,H). Each frame is a maximum projection of 16 optical slices at 0.5 μm step size.



Movie 4. 120 min of nuclear movement in a SiR-Actin and Hoechst labeled wild type (w^{1118}) stage 10B egg chamber. Images were taken every 15 min. Each frame is a maximum projection of 5 optical slices at 0.5 μm step size. This is an example of the type of data we used to calculate the nuclear movement trajectories and distances shown in Fig. 8K. In this example, we used ImageJ (Fiji v.1.53q) to calculate the cell centroids (black dots) using the actin images and the nuclear centroids (cyan dots) using the nuclear images for each frame. For the data in Fig. 8K, only the 0 min and 90 min time points were used to calculate trajectory and distance (see Methods for details). Thus, in our quantification, we did not track the specific paths that the nuclei take like we did in this example. More detailed tracking of nuclear paths in future experiments might generate novel insights into how the actin cable arrays guide nuclear movement.